Journal of Thermal Engineering, Vol. 4, No. 3, pp. 2018-2036, April, 2018
Yildiz Technical University Press, Istanbul, Turkey

EFFECTS OF HEATER DIMENSIONS ON NANOFLUID NATURAL CONVECTION IN A HEATED INCINERATOR SHAPED CAVITY CONTAINING A HEATED BLOCK

Mohamed Ammar Abbassi[1*], Ridha Djebali[2], Kamel Guedri[3]

ABSTRACT

The present work reports a numerical study of natural convection in an incinerator shaped enclosure with a localized heated source situated at the bottom. Lattice Boltzmann Method (LBM) is used to simulate nanofluid (water-Al_2O_3) flow and heat transfer. Simulations have been carried out for the pertinent parameters: Rayleigh number ($Ra=10^3-10^6$), solid volume fraction $0 \le \phi \le 6\%$ relative heat source high ($0 \le \delta \le 0.5$), relative heat source width ($0.02 \le \varepsilon \le 0.8$), and inclination angle of the incinerator ($0 \le \gamma \le 360°$). The comparison of the obtained results is in excellent agreement with results from literature. It may be noted that the Rayleigh number, the solid volume fraction, the heat source tallness enhances the heat transfer and influences the flow pattern and the thermal structures. However for the relative heat source width plays opposite role for values superior to 0.4.

Keywords: *Heat Transfer, Incinerator Geometry, Lattice Boltzmann Method, Natural Convection, Nanofluid*

INTRODUCTION

Augmentation of heat transfer is an important goal in generating energy systems. Different mechanisms of heat transfer enhancement have been highlighted in the literature focusing mainly on modifying the geometry, swirl flow devices, use of porous media, partitioned cavities and other techniques, which are well documented [1]. Recently, an innovative way of heat transfer enhancement is the use of nano-suspensions (particles, fibers) of relatively higher thermal conductivities suspended in the base fluids. Bergles [2] classified the techniques of heat transfer enhancement as active or passive. Active methods require external power to maintain the enhancement mechanism, whereas passive enhancement techniques don't require external power. The addition of nano-sized particles to a base fluid in order to enhance its thermal conductivity is classified among the passive enhancement techniques. The obtained solution is called nanofluid which is introduced first by Choi [3]. Nanofluids are referred to the fluids with suspensions of nanoparticles having a diameter below 100nm. According to Mahbubul et al. [4], nanofluids is a solid-liquid mixture which consists of nanoparticles and a base liquid. Nanoparticles are basically metal (Cu, Ni, Al, etc), oxides (Al_2O_3, TiO_2, CuO, SiO_2, Fe_2O_3, Fe_3O_4, $BaTiO_3$,etc) and some other compounds (AIN, SiC, $CaCO_3$, graphene, etc) and base fluid usually include water, ethylene glycol, propylene glycol, engine oil, etc. Compared to other techniques used for enhancing heat transfer in practical applications, nanofluids have the advantage of behaving like pure fluids, because of the small size of nanoparticles. This technique can be used for the thermal machines which will be constructed in the future or even for the ones which are already functioning with little modifications. A review of recent research made with nanofluids can be found in [5]. Natural convection heat transfer due to a localized heat source in complex geometries is ubiquitous in the majority of industrial systems.

It has been studied extensively because of its interest in many practical systems, including cooling of electronic equipments, material processing, chimneys, furnaces, heat exchangers, solar energy collectors, nuclear engineering, fire research, building engineering and geophysical flows. Ben Cheikh et al. [6] investigated numerically two-dimensional natural convection flow of a dielectric fluid in a square inclined enclosure with a fin placed on the hot wall. They found that for small enclosure inclination angles and moderate values of Rayleigh number (Ra), the flow is steady and mainly constituted by two counterclockwise eddies. For higher values of Ra, secondary eddies were observed between the fin sides and the lower passive walls. They also demonstrated that the inclination angle controls the transition to the unsteady state. Abbassi et al.[7] made a numerical studied of nanoparticle Brownian motion and magnetic field effects by natural convection in a nanofluid-filled open cavity with non uniform boundary condition. The Lattice Boltzmann Method is used as a simulation tool. The numerical

This paper was recommended for publication in revised form by Regional Editor Jaap Hoffman Hoffman
[1]Materials, Energy and Renewable Energies (MEER), University of Gafsa, Tunisia.
[2]ISLAIB – Béja 9000, University of Jendouba, Tunisia
[3]Mech. Eng. Dep., College of Eng. and Islamic Architecture, Umm Al-Qura University, Saudi Arabia.
**E-mail address: abbassima@gmail.com*
Manuscript Received 28 October 2016, Accepted 17 December 2016

results show a decrease in heat transfer with an increase in particle volume fraction. In addition, it is observed that the Brownian motion greatly influences the heat transfer rate depending on the Hartmann number, Rayleigh number and nanoparticle volume fraction. Öztop et al. [8] reviewed the effects of curvilinear boundaries on heat and nanofluid flow by natural convection. They clarified the energetic value of achieving highly efficient energy transport at reduced cost via different approaches, including change in the structural configuration of thermal systems and using nanofluids. They observed that curvilinear surface is the main effective parameter on heat and fluid flow in a nanofluid filled enclosure due to natural convection. Moumni et al. [9] investigated numerically two-dimensional mixed convection fluid flow and heat transfer of water–nanofluids in a two-sided facing lid-driven cavity. Two discrete heat sources are located at the bottom wall of the enclosure. The governing equations are solved using a second order accurate finite volume approach. It was found that significant heat transfer enhancement can be obtained. The addition of nanoparticles decreases the fluid motion and increases the heat transfer rate considerably. The location of the two heat sources also affects the average Nusselt number. The latter increases as the locations of the two heat sources move respectively toward the left and the right walls. Mahfoud and Bendjaghloli [10] studied natural convection in a truncated cone filled with Cu-water nanofluid. They used the finite volume approach to solve the governing equations coupled with the SIMPLE algorithm. Their results showed an enhancement in cooling system when using a nanofluid. Also they demonstrated that the inclination angle of inclined sidewalls and heat source length affect the heat transfer rate and the maximum temperature. Hassan [11] investigated by the FVM heat transfer inside horizontal and vertical enclosures filled with Cu–water nanofluid. A heat sink with rectangular fins represents the base plate of the enclosure where it is heated by a discrete heat source at the bottom of the heat sink. The effect of volume fraction and diameter of the Cu nanoparticles on the average Nusselt number of the heat source is studied. He demonstrated that the average Nusselt number on the heat source increases with the increase of Rayleigh number and nanoparticle volume fraction and with decrease nanoparticle diameter. Using nanofluid increases the number of circulating cells and decreases their size compared with enclosure without nanofluid. The temperature of the heat source decreases when increasing Rayleigh number, increasing of nanoparticle volume fraction and with decrease of nanoparticle diameter. Öztop et al.[12] presented an exhaustive review of natural convection heat transfer and fluid flow in different enclosures with localized heat sources. The common objective of their review work is to investigate the effects of type and location of local heat sources as well as the effects of the different configurations and boundary conditions on the enclosed fluid/nanofluid flow and heat transfer. Kaluri et al.[13] studied laminar natural convection in a square cavity with distributed heat sources by the help of heatline and streamline approach. They considered four different cases, depending on the location of the heat sources on the walls of the cavity. They showed that the used method is found to be adequate to visualize and understand heat energy distribution and thermal mixing occurring inside the considered cavity. Multiple heat sources are also studied by Aminossadati and Ghasemi [14], they considered the problem of natural convection in a 2D cavity filled with nanofluid. Two pairs of heat source–sink are situated on the bottom wall of the cavity while the other walls are thermally insulated. The governing differential equations are solved by the control volume approach. The main goal of their study was to compare the heat transfer performance at different Rayleigh numbers and solid volume fraction of the nanofluid. The results show that regardless of the position of the pairs of source–sink, the heat transfer rate increases with an increase of the Rayleigh number and the solid volume fraction. Mussa et al. [15] studied numerically natural convection in an enclosure using Cubic-Interpolated-Pseudo-Particle (CIP) lattice-Boltzmann method. A D2Q9 lattice model was coupled with the D2Q4 lattice model to represent density and internal energy distribution functions, respectively.

The effect of the Rayleigh number on the flow pattern is studied. The enclosure is filled with air heated by a small localized heat source at two different positions on the bottom wall. Their results showed that natural convection increases with the Rayleigh number and heat source locations. Corvaro and Paroncini [16] analyzed experimentally convective heat transfer generated by a source with three different heights. The source is located in the middle of a square enclosure. The experimental analysis was carried out using holographic interferometry for the study of heat transfer and a 2D-PIV system to analyze the dynamic behavior of the phenomenon. The comparison is based both on the evaluation of the Nusselt number at different Rayleigh numbers and the study of the velocity fields at the same Rayleigh numbers in different configurations. Their experiments showed that the natural convective heat transfer worsens with the source height increase. In the last decades, the Lattice Boltzmann Method (LBM) is emerged as a powerful numerical technique, based on kinetic theory, to simulate fluid flow, heat

and mass transfer. It has become a novel alternative to conventional Computational Fluid Dynamics (CFD) solvers like Finite Difference Method (FDM), Finite Element Method (FEM) and Finite Volume Methods (FVM) for solving the Navier–Stokes Equations (NSE) [17]. The advantages of LBM include simple calculation procedures and ease in implementation of boundary conditions. It is well suitable for parallel computation, ease and robust in handling of multiphase flow and can be applied for complex geometries [18, 19]. Moreover, when using LBM, the coupling between pressure and velocity field is avoided. In conventional classical methods this linkage is handled by algorithms such as SIMPLE, SIMPLER [20] and others which are CPU time consumers. Another advantage it can capture turbulence without any turbulence models [19]. The main aim of the present paper is to investigate numerically the heat transfer rate and the fluid flow in nanofluid filled incinerator shaped geometry. A heated block is situated on the bottom wall of the incinerator, whereas the vertical walls are considered cold and the top wall is supposed to be adiabatic. The LB method is applied to solve the coupled momentum and energy equations. The grid independency test and the validation of the present model are conducted on simple cavity cases. The effects of the main parameters (Rayleigh number, solid volume fraction, inclination angle, heat source width, heat source height, and heat source position) on flow, thermal fields and Nusselt number are presented and discussed.

PHYSICAL MODEL AND MATHEMATICAL FORMULATION

Figure 1 shows the considered two-dimensional problem with boundary conditions and coordinate system. It is an incinerator shaped enclosure of length L and height H (ABCDEFGH). The heat source (A1B1C1D1) at high temperature Th is located at the bottom surface of the cavity and has the width a and height b. The other parts of the bottom wall and the ceiling are considered adiabatic. The remaining walls of the cavity are cold. To make a straightforward study, the following assumptions are retained. The flow is steady, laminar and incompressible; all the thermophysical properties of the fluid are constant, except for the density in the buoyancy term which follows the Boussinesq approximation. The base fluid and the nanoparticles are assumed to be in thermal equilibrium and the nanofluid is Newtonian. The nanoparticles are supposed to be of spherical shape and the radiation effects are neglected.

The non-dimensional form of the problem variables are implemented in the following:

$$U_0 = \frac{\alpha}{H}; X,Y = \frac{x,y}{H}; U,V = \frac{u,v}{U_0}; \theta = \frac{T-T_c}{T_h-T_c}; \tau = \frac{tU_0}{H} \text{ and } P = \frac{p+\rho_0 gy}{\rho_{nf}U_0^2} \tag{1}$$

Based on the above assumptions, the dimensionless governing equations can be expressed in the incompressible unsteady form as follows:

$$\frac{\partial U}{\partial X} + \frac{\partial V}{\partial Y} = 0 \tag{2}$$

$$\frac{\partial U}{\partial \tau} + \frac{\partial (UU)}{\partial X} + \frac{\partial (UV)}{\partial Y} = -\frac{\partial P}{\partial X} + \Pr \frac{\rho f}{\rho nf} \frac{1}{(1-\varphi)^{2.5}} \left(\frac{\partial^2 U}{\partial X^2} + \frac{\partial^2 U}{\partial Y^2} \right) \tag{3}$$

$$\frac{\partial V}{\partial \tau} + \frac{\partial (UV)}{\partial X} + \frac{\partial (VV)}{\partial Y} = -\frac{\partial P}{\partial Y} + \Pr \frac{\rho f}{\rho nf} \frac{1}{(1-\varphi)^{2.5}} \left(\frac{\partial^2 V}{\partial X^2} + \frac{\partial^2 V}{\partial Y^2} \right) + \Pr Ra \frac{\rho f}{\rho nf} \left(1-\varphi + \frac{\rho_S \beta_S}{\rho_f \beta_f} \varphi \right) \theta \tag{4}$$

$$\frac{\partial \theta}{\partial \tau} + \frac{\partial (U\theta)}{\partial X} + \frac{\partial (V\theta)}{\partial Y} = \frac{\alpha_{nf}}{\alpha_f} \left(\frac{\partial^2 \theta}{\partial X^2} + \frac{\partial^2 \theta}{\partial Y^2} \right) \tag{5}$$

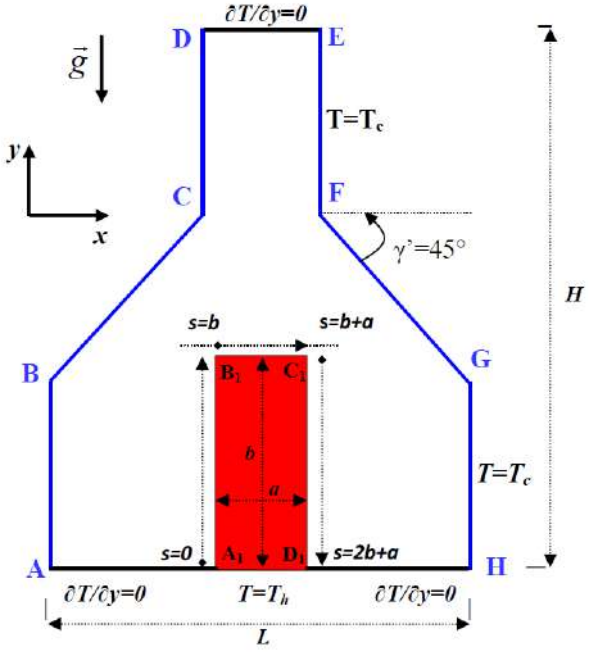

Figure 1. Geometry of the incinerator

Accordingly, the hot block dimensionless width and height are expressed as $\delta = b/H$ and $\varepsilon = a/L$ respectively. Besides, natural convection problems are described by two non-dimensional monitoring parameters, namely the Rayleigh number *Ra* and the Prandtl number *Pr* expressed as:

$$Ra = \frac{g\beta\Delta T\, H^3}{\upsilon_f \alpha_f} \; and \; \Pr = \frac{\upsilon_f}{\alpha_f} \tag{6}$$

Where υ_f is the kinematic viscosity, α_f the thermal diffusivity and β is the nanofluid thermal expansion coefficient; g is the gravitational acceleration and $\Delta T = T_h - T_c$ the temperature difference between the hot source and the cold wall.

LATTICE BOLTZMANN METHOD

The main variable in LBM algorithm is the density distribution function $f_i(x,t)$ of the fluid pseudo-molecules that has lattice velocity $\boldsymbol{c}_i$ at location $\boldsymbol{x}$ at a time t. The lattice Boltzmann equation with Bhatnagar-Gross-Krook (BGK) collision mode, for incompressible problems, uses two distribution functions, f and g, for the flow and temperature fields respectively. For the flow field, the discretized LBM equations can be written as [7]:

$$f_i\left(\boldsymbol{x} + c_i\Delta t, t + \Delta t\right) - f_i\left(\boldsymbol{x},t\right) = -\frac{1}{\tau_\upsilon}\left[f_i\left(\boldsymbol{x},t\right) - f_i^{eq}\left(\boldsymbol{x},t\right)\right] + \Delta t F_i \tag{7}$$

For the temperature field

$$g_i\left(\boldsymbol{x} + c_i\Delta t, t + \Delta t\right) - g_i\left(\boldsymbol{x},t\right) = -\frac{1}{\tau_\alpha}\left[g_i\left(\boldsymbol{x},t\right) - g_i^{eq}\left(\boldsymbol{x},t\right)\right] \tag{8}$$

where Δt denotes the lattice time step which is set to unity and τ_υ, τ_α are the relaxation times for the velocity and temperature fields, respectively. f_i^{eq}, g_i^{eq} are the local equilibrium distribution functions (Eq. (9)) that have an appropriately prescribed functional dependence on the local hydrodynamic properties and F_i is an external force term. The left-hand side of Eq. (7) is often called streaming or propagation and accounts for the migration of the

fluid molecules from one grid point to its neighboring nodes. The right hand side is the collision part which models the relaxation process of the molecules towards the local equilibrium distribution f_i^{eq}, namely the truncated Boltzmann distribution when using the BGK collision model.

$$f_i^{eq} = \omega_i \rho \left(1 + \frac{\mathbf{c_i}.\mathbf{u}}{c_s^2} + \frac{(\mathbf{c_i}.\mathbf{u})^2}{2c_s^4} - \frac{\mathbf{u}^2}{2c_s^2} \right); \; g_i^{\mathrm{eq}} = \omega_i \theta \left(1 + \frac{\mathbf{c_i}.\mathbf{u}}{c_s^2} \right) \tag{9}$$

where u and ρ are the macroscopic velocity and density, respectively, $c = \Delta x / \Delta t$ is the lattice speed, Δx is lattice space and similar to lattice time step is equal to unity, ω_i is the weighting factor for flow, and temperature. The double populations D2Q9-D2Q9 thermal model is used in this study. Thus, the weighting factors and the discrete particle velocity vectors are given as follows:

$$\omega_0 = 4/9, \omega_{i=1-4} = 1/9, \; \omega_{i=5-8} = 1/36 \tag{10}$$

$$\vec{c}_i = \begin{pmatrix} c_{x,i} \\ c_{y,i} \end{pmatrix} = c. \begin{pmatrix} 0,1,0,-1,0,1,-1,-1,1 \\ 0,0,1,0,-1,1,1,-1,-1 \end{pmatrix} \text{ and } \quad c_s = c/\sqrt{3} \tag{11}$$

The SRTs of the standard LB equations are linked to the diffusion parameters as: $\upsilon = (2\tau_\upsilon - 1)c^2 \Delta t / 6$ and $\alpha = (2\tau_\alpha - 1)c^2 \Delta t / 6$

LATTICE BOLTZMANN METHOD FOR NANOFLUID

The nanofluid behavior is assumed to be similar to a single phase fluid. The effective density (ρ_{nf}), heat capacitance $(\rho C_p)_{nf}$, the thermal expansion coefficient (β_{nf}), nanofluid thermal diffusivity (α_{nf}), nanofluid viscosity (μ_{nf}), and nanofluid thermal conductivity (k_{nf}) are respectively defined as follows:

$$\rho_{nf} = (1-\phi)\rho_f + \phi\rho_p \tag{12}$$

$$(\rho C_p)_{nf} = (1-\phi)(\rho C_p)_f + \phi(\rho C_p)_p \tag{13}$$

$$(\rho\beta)_{nf} = (1-\phi)(\rho\beta)_f + \phi(\rho\beta)_p \tag{14}$$

$$\alpha_{nf} = \frac{k_{nf}}{(\rho C_p)_{nf}} \tag{15}$$

$$\mu_{nf} = \mu_f (1-\phi)^{-2.5} \tag{16}$$

$$k_{nf} = k_f \frac{k_P + 2k_f - 2\phi(k_f - k_P)}{k_P + 2k_f + \phi(k_f - k_P)} \tag{17}$$

BOUNDARY CONDITIONS

Regarding the boundary conditions of the flow field, the solid walls are assumed to be no slip.

Incinerator walls *AB*, *BC, CD*, *DE, EF, FG, GH, HA*: $U=V=0$

Incinerator walls *AB*, *BC, CD, EF, FG, GH*: $T=T_c$

Incinerator walls *DE, HD*$_1$, *A*$_1$*A*: $\partial T / \partial y = 0$

Heated block walls, A_1B_1 , B_1C_1 ,C_1D_1,D_1A_1: $U=V=0$, $T=T_h$

Thus, by applying the bounce-back scheme at the boundary nodes (Figure 2), the outer distribution functions from the domain are known from the streaming process and the inner ones are determined as follows for the flow BCs:

AB, *CD*, C_1D_1: $f_1=f_3, f_5=f_7, f_8=f_6$,

BC: $f_1=f_3, f_4=f_2, f_8=f_6$,

DE : $f_4=f_2, f_8=f_6, f_7=f_5$,

EF, *GH*, A_1B_1: $f_3=f_1, f_7=f_5, f_6=f_8$,

FG: $f_3=f_1, f_4=f_2, f_7=f_5$

and *AH*, B_1C_1: $f_2=f_4, f_5=f_7, f_6=f_8$.

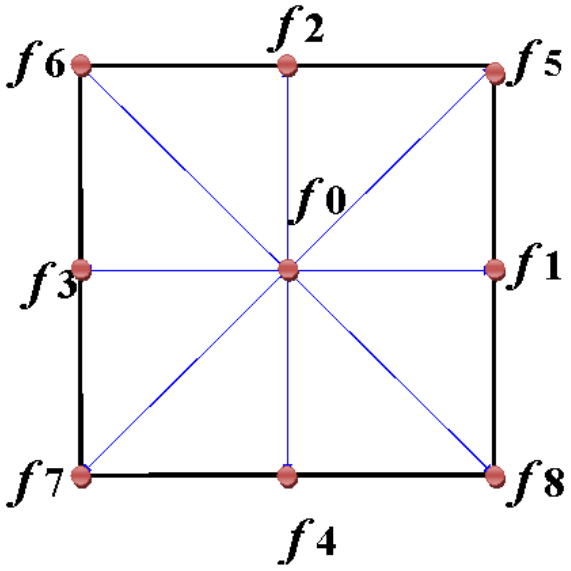

Figure 2. Domain boundaries and direction of streaming velocities, D2Q9

For the thermal boundary conditions we have:

AB, *CD*: $g_1=-g_3, g_5=-g_7, g_8=-g_6$,

BC: $g_1=-g_3, g_4=-g_2, g_8=-g_6$,

DE: $g_{4,n}=g_{4,n-1}, g_{7,n}=g_{7,n-1}, g_{8,n}=g_{8,n-1}$,

EF, *GH*: $g_3=-g_1, g_7=-g_5, g_6=-g_8$,

FG: $g_3=-g_1, g_4=-g_2, g_7=-g_5$,

A_1B_1: $g_3= 2/9-g_1, g_4=2/9-g_2, g_7=2/9-g_5$,

B_1C_1: $g_1= 2/9-g_3, g_2=2/9-g_4, g_5=2/9-g_7$,

C_1D_1: $g_2= 2/9-g_4, g_5=2/9-g_7, g_6=2/9-g_8$

and *AH*: $g_{2,n}=g_{2,n-1}, g_{5,n}=g_{5,n-1}, g_{6,n}=g_{6,n-1}$.

NON DIMENSIONAL PARAMETERS

In the LBM simulations the Rayleigh number, Prandtl number and Mach number are assigned constants values therefore the viscosity and thermal diffusivity are calculated from the definition of these non dimensional parameters.

$$\upsilon = n\ Ma\ c_s \sqrt{\frac{\mathrm{Pr}}{\mathrm{Ra}}} \tag{18}$$

where n is the number of lattice nodes in y-direction.

To insure an incompressible flow the Mach number was chosen as $Ma \le 0.1$.

transfer rate on the heat source is described by the Nusselt number Nu which is given by:

$$Nu_l = \frac{hH}{k_f} \tag{19}$$

where the heat transfer coefficient is computed from:

$$h = \frac{q_w}{T_h - T_C} \tag{20}$$

The thermal conductivity of the nanofluid is expressed as:

$$k_{nf} = -\frac{q_w}{\partial\theta / \partial x} \tag{21}$$

and using the dimensionless quantities, the local Nusselt number along the left wall can be written as:

$$Nu_l = -\frac{k_{nf}}{k_f}\left(\frac{\partial\theta}{\partial X}\right)\Big|_{Heat\ \text{Source Walls}} \tag{22}$$

The average Nusselt number is obtained by integrating the local Nusselt number along the heat source:

$$\overline{Nu_l} = -\frac{1}{b}\int_{A_1}^{B_1}\frac{k_{nf}}{k_f}\left(\frac{\partial\theta}{\partial X}dY\right)\Big|_{X=(L-a)/2} - \frac{1}{a}\int_{B_1}^{C_1}\frac{k_{nf}}{k_f}\left(\frac{\partial\theta}{\partial Y}dX\right)\Big|_{Y=b} - \frac{1}{b}\int_{C_1}^{D_1}\frac{k_{nf}}{k_f}\left(\frac{\partial\theta}{\partial X}dY\right)\Big|_{X=(L+a)/2} \tag{23}$$

GRID INDEPENDENCE STUDY AND VALIDATION

To ensure the grid independence we examine the sensitivity of our results for different uniform grids: 50×50, 80×80, 100×100, 120×120, 150×150, 200×200 and 250×250 and for all the studied Rayleigh numbers. For each Ra value, if the tested quantity converges, the grid size is adopted. This idea avoids time consuming for lower monitoring parameters (Ra) which may be pointless. The results of simulations for the tested grids are presented in Table 1.

Table 1. Grid independency test: Calculated average Nusselt number on the heat source left side for Rayleigh numbers Ra = 10^5 , δ=0.4, ε=0.2 and γ= 0°.

Ra/ Grid	50	80	100	120	150	200	250
10^3	1.37029	1.40321	1.41664				
10^4	1.52299	1.54700	1.55614	1.56288			
10^5	3.11312	3.14092	3.14398	3.14433	3.14364		
10^6	3.95367	4.13062	4.17767	4.20729	4.24371	4.31071	4.33071

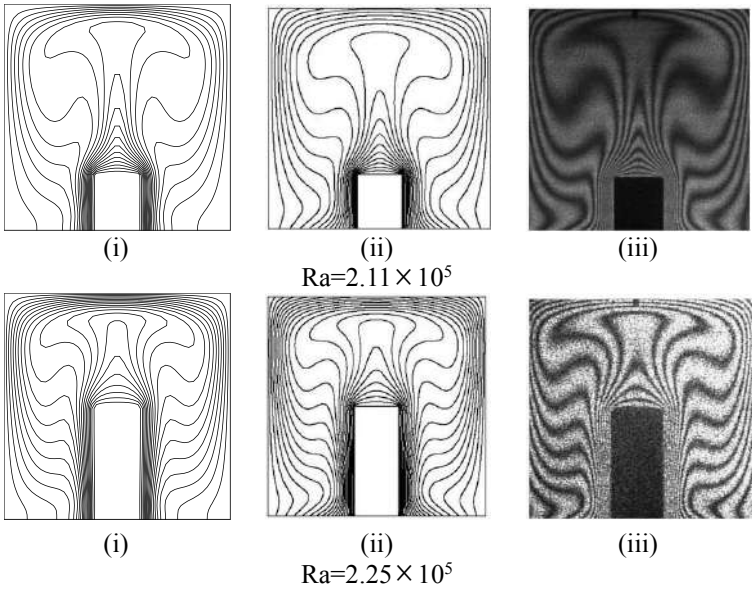

Figure 3. Comparison between (i) Present code, (ii) CIP thermal lattice-Boltzmann method [15] and (iii) experimental study (Ra = 2.02×10^5 and $\delta=0,5$)

It may be observed a convergence for low Rayleigh numbers at coarser grids. This issue has been discussed and adopted by Djebali et al. [18]. The retained grids are 100×100 for Ra≤10^4, 120×120 for Ra=10^5 and 200×200 for Ra=10^6. A comparison between present code, the CIP thermal LB method used by Mussa et al. [15] and the numerical (using Fluent code) and experimental results presented in [16] for the cases of square cavity at Ra = 2.02×10^5 and Ra=1.38×10^5 is shown in

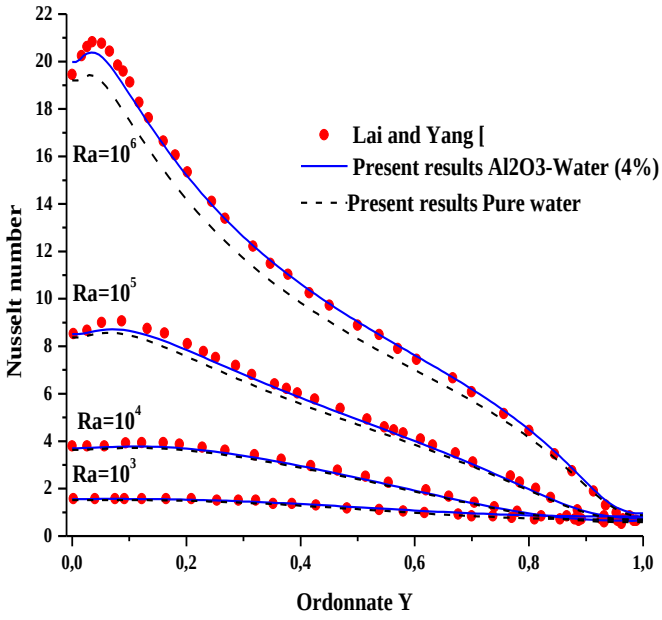

Figure 4. Nusselt number distribution along the hot wall for Ra=10^3- 10^6 at a solid volume fraction $\phi=0-4\%$

Figure 3 quantitatively, our results agree well with the literature findings for the temperature contours plots. Besides, Figure 4 shows the local Nusselt number computed for four Rayleigh numbers (*Ra* = 10^3- 10^6) and

for two values of the solid volume fraction $\phi = 0\%$ and $\phi = 4\%$. Quantitatively, compared with results by Lai and Yang [22] who used the Lattice Boltzmann Method, in this case also excellent results are found.

RESULTS AND DISCUSSIONS

In this paper natural convection inside an incinerator shaped enclosure filled with Al_2O_3-water nanofluid and having a hot rectangular source situated in the bottom face have been investigated. Steady state results are presented for different dimensionless parameters: Rayleigh number $(10^3 \le Ra \le 10^6)$,nanoparticle volume fraction $(0 \le \phi \le 6\%)$ relative hot source height $(0 \le \delta \le 0.5)$, relative hot source width $(0 \le \varepsilon \le 0.8)$, and inclination angle of the incinerator $(0 \le \gamma \le 360°)$. Results are presented as streamlines, isotherms, and average Nusselt numbers.

EFFECT OF RAYLEIGH NUMBER (Ra)

Figure 5 shows the effect of Rayleigh number on streamlines and isotherms inside an incinerator including a hot rectangular heat source (ε=0.2, δ=0.5) and filled with pure fluid (water) and nanofluid with =4%. x=0.5 represents a symmetric plane for both isotherms and streamlines. For low Rayleigh numbers ($Ra=10^3$-10^4), isotherms are parallel to the three faces of the hot source and are perpendicular to the bottom surface of the incinerator and horizontal thermal like stratification is formed around the heater. Streamlines form two counter rotating big cells from either part of the heater. Increasing Rayleigh number to $Ra=10^5$, convection currents are more expressed and the isotherms are slightly tightened near hot walls to form a thermal boundary layer and the stratification is distorted. The streamlines still form a symmetric cells more elongated to the top due to the ascendant fluid motion and are occupying the whole medium below y=0.7.

For $Ra=10^6$ the symmetry of the flow and thermal behavior is broken. One can remark the formation of two new counter rotating cells of different sizes. These two cells are formed due to the like Rayleigh-Bénard convection that hold at the upper wall of the heat source where the upper corner of the two big cells serve as moving (lid) boundary conditions to the formations of the small cells.

It is also worth to mention that the big rotation cells take the geometric forms of the surrounding space due to the intensified pressure. For the isotherms, boundary layers are clearly formed near the isotherm (hot and cold) walls and a like vertical stratification is formed between vertical walls of the heater and those of the incinerator. The former two small cells intensify the heat transfer rate from the upper heater wall. The overall heat transfer from the heated block is 4.034, 4.182, 6.909 and 14.222 for pure water and 4.680, 4.772, 7.1952 and 15.266 for nanofluid at $Ra=10^3$, 10^4, 10^5, and 10^6 respectively. Thus, increasing the Rayleigh number from 10^3 to 10^6 and the solid volume fraction from 0 to 6% enhances about three times the heat transfer.

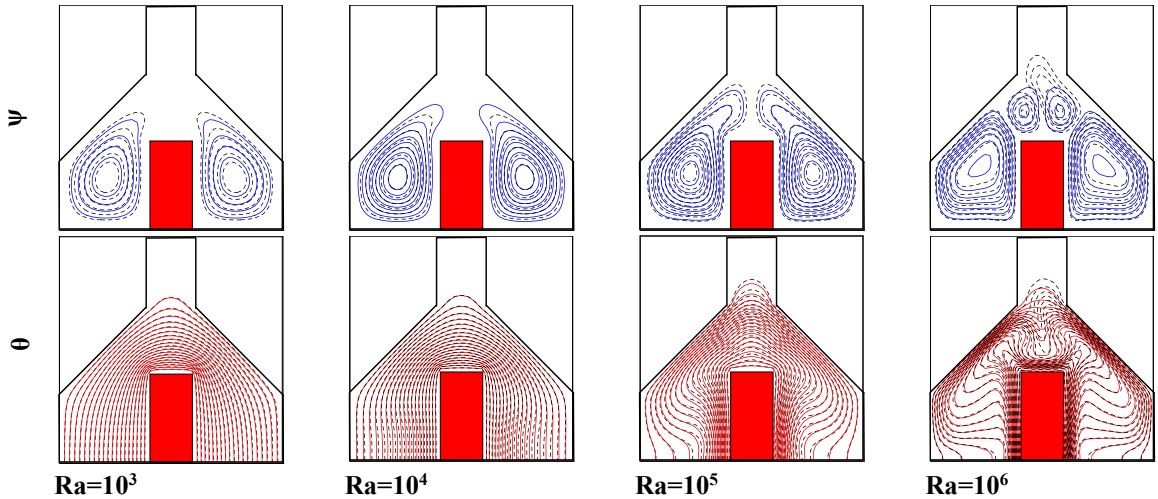

Figure 5. Effect of Rayleigh number on streamlines and isotherms inside the incinerator for δ=0.4, ε=0.2 and γ= 0° (—Base fluid; ---nanofluid, $\phi = 4\%$).

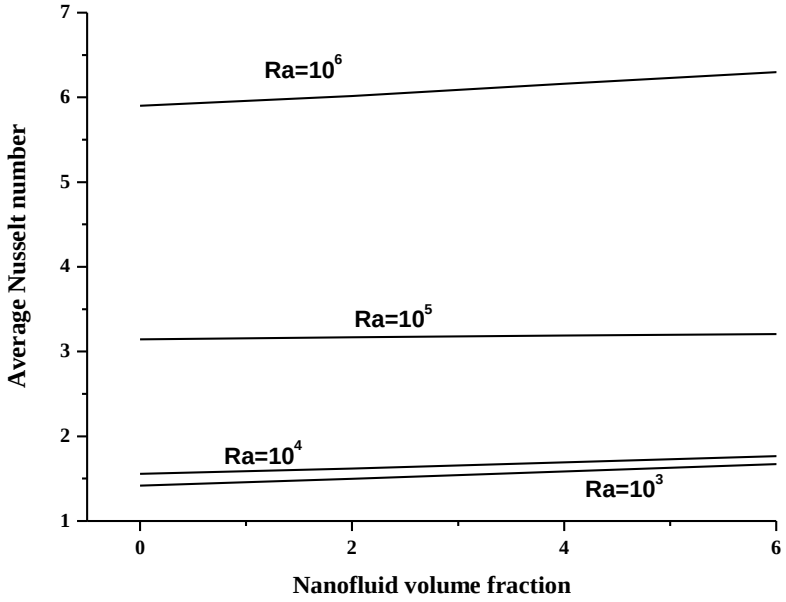

Figure 6. Nanoparticle volume fraction effect on average Nusselt number on the heat source left side for different Rayleigh numbers and δ=0.4, ε=0.2 and γ= 0°.

EFFECT OF THE NANOPARTICLE VOLUME FRACTION

For all Rayleigh numbers considered in this study heat transfer is obviously increased as the solid volume fraction increases. At low Rayleigh numbers ($Ra=10^3$-10^4), the addition of nanoparticles augments the heat transfer. However, if the Rayleigh number increases ($Ra=10^5$-10^6), the addition of nanoparticles leads to a heat transfer rise on the heater vertical side walls whereas, a heat transfer reduction on its top wall is remarked. This pattern can be explained by the formation of two eddies placed at the heater top wall which decrease fluid flow motion to the incinerator top and consequently reduces the heat transfer. Besides, it can be seen from Figure 5 that the addition of nanoparticles does not affect the global dynamic and thermal structures. Figure 6 depicts the wall average Nusselt number at the left (or the right) of the hot block as a function of the Rayleigh number variation for $10^3 \leq Ra \leq 10^6$. First, one can see easily the rapid variation of the average Nusselt number with the Rayleigh number rise at constant solid volume fraction ϕ; and second the average Nusselt number increases by increasing the volume fraction ϕ of nanoparticles. However, for the top facet average Nusselt number a reduction is observed by increasing Ra to 10^5. This is explained by the fact that the ascendant flow near vertical walls creates a convective boundary layer parallel to hot walls which augments the heat transfer. These currents drive with them the fluid from either side of the heater top wall and its boundary layers become more spaced and the cells from either part of the hot block become more elongated to strangle the flow above the top wall. These two effects induce the decrease of heat transfer due to the heater top wall. Besides, for $Ra=10^6$, the flow is characterized by the appearance of two new cells of different dimensions above the heater top wall. The corresponding Nusselt number is significantly increased compared to $Ra=10^5$ because the counter rotating two small cells drive with them the cold fluid from the incinerator neck. The tendency is same for all nonzero solid volume fractions.

EFFECT OF THE INCINERATOR TILT ANGLE

Figure 7a) presents the effect of the inclination angle (γ) on the streamlines and isotherms for two volume fractions $\phi = 4\%$ (dashed lines) and $\phi = 0\%$ (solid lines). The Rayleigh number is chosen equal to $Ra=10^5$, the heater height is chosen 0.4, and the tilt angle varies from 0° to 360°.

For $\gamma = 60°$, the dynamic structure is typified by three cells (eddies) of different forms and dimensions at the left, top and right of hot block. The left and top cells are linked and are counter clockwise rotating. The right cell takes the form of the surrounding space and is clockwise rotating. Compared to the γ=0° case, the thermal

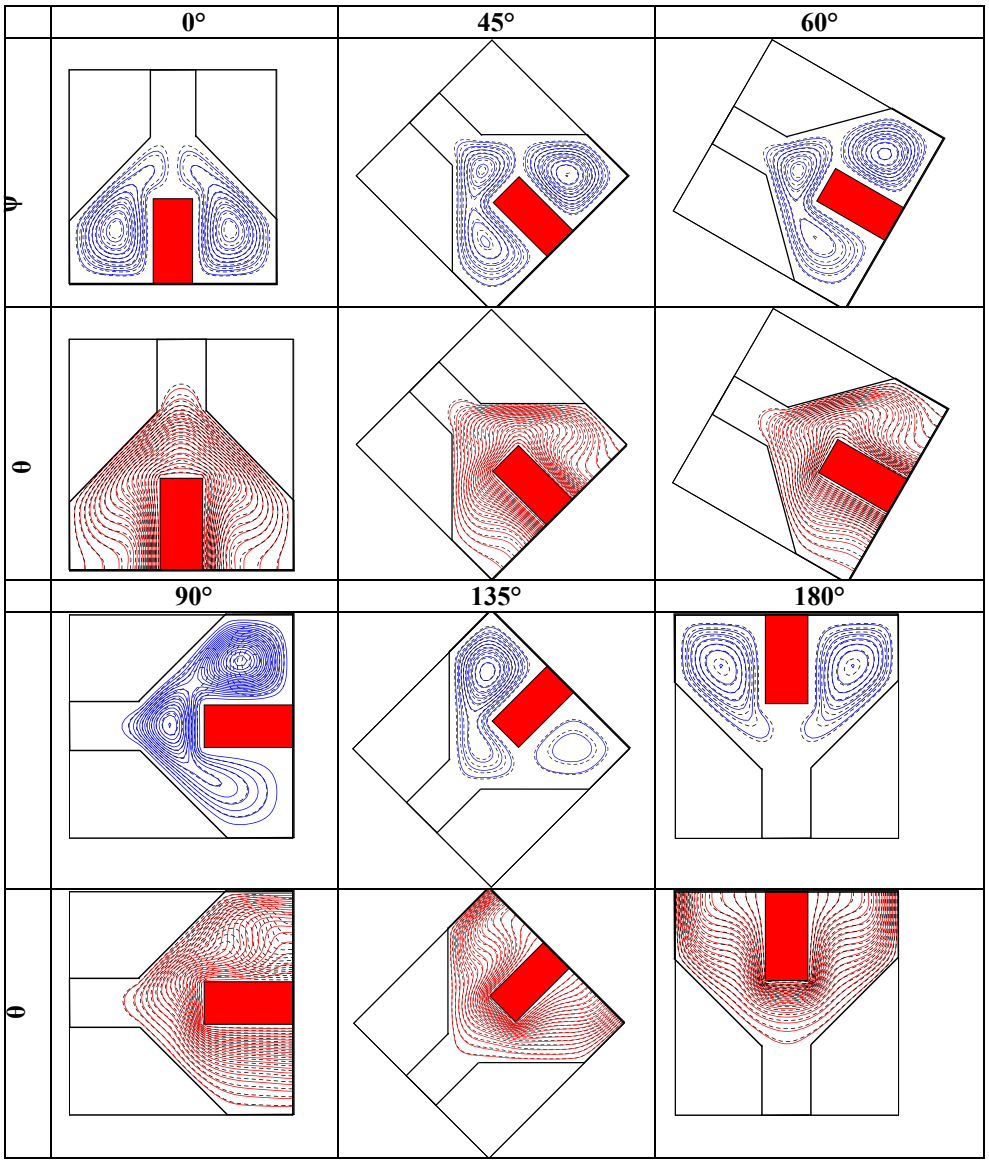
0°
45°
60°
ψ
θ
90°
135°
180°
θ

a)

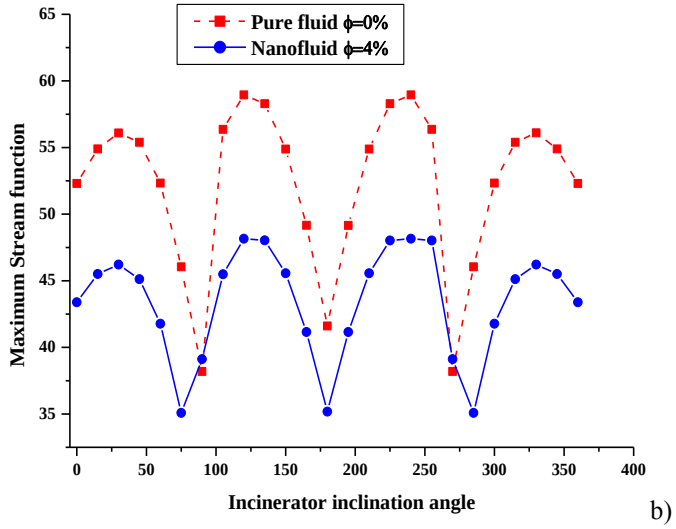
Pure fluid ϕ=0%
Nanofluid ϕ=4%
Maximum Stream function
Incinerator inclination angle
65
60
55
50
45
40
35
0
50
100
150
200
250
300
350
400

b)

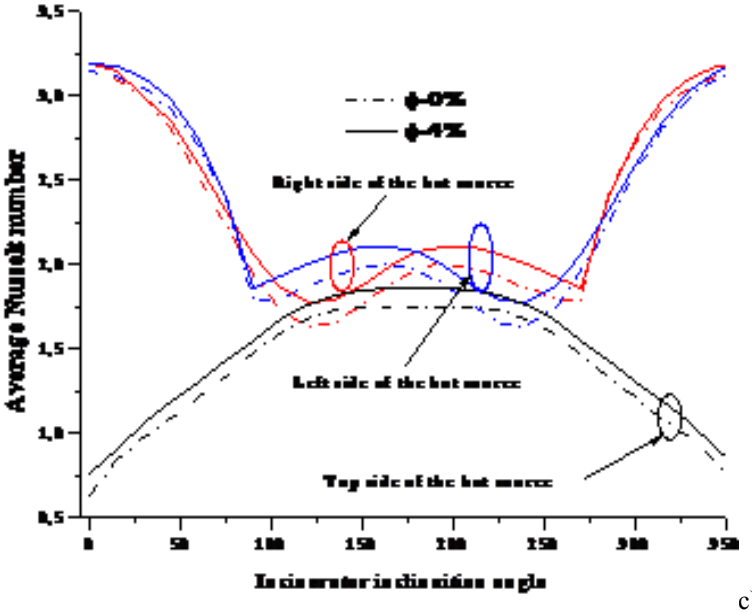

c)

Figure 7. a) Effect of inclination angle γ on streamlines and isotherms for Ra = 10^5 and δ=0.4, ε=0.2 (—Base fluid; ---nanofluid) b) Effect of inclination angle γ on stream function maximum for Ra = 10^5 and δ=0.4, ε=0.2 (—Base fluid; ---nanofluid) c) Effect of inclination angle on average Nusselt number on the heat source sides (— Base fluid; ---nanofluid,).

structure has changed widely at the right of the hot block. Besides, one can say that the effect of adding nanosuspensions does not affect the pure dynamic and thermal structure for γ=60° tilting case. For a quarter turn rotation ($\gamma = 90°$), the streamlines for the pure fluid are formed by two eddies, whereas for the nanofluid these two eddies are merged on one big eddy occupying the whole medium. Increasing continuously the tilt angle, we obtain again two eddies for the pure fluid and the nanofluid and the head of the top cell begins to detach to fuse with the right cell and form a large cell extended from right to the top of the heater. The large cell dimension diminishes as the tilt angle approaches 180° where we obtain symmetric acting two equal cells.

Figure 7b) depicts the effect of the incinerator inclination angle on the absolute stream function maximum for pure fluid and nanofluid at $\phi = 4\%$ and for Ra=10^5. It can be seen easily that for the studied inclination angles, the maximum of the stream function in the case of pure fluid is almost higher than in the case of the nanofluid. This behavior can be explained by the augmentation of friction when nanoparticles are added ($\mu_{nf} > \mu_f$).

Figure 7c) presents the effect of inclination angle average Nusselt number on the heater three hot facets for both cases of base fluid and nanofluid with $\phi = 4\%$. In the case of the top side of the heater source we can distinguish three zones: for $0 \le \gamma \le 150°$ the average Nusselt number increases as the inclination angle increases. For $150° \le \gamma \le 220°$ the average Nusselt number is nearly constant with the inclination angle. And for $220° \le \gamma \le 360°$ the average Nusselt number decreases with the inclination angle.

The Nusselt number in the case of the right and left sides decreases with increasing inclination angle for the range $0° \le \gamma \le 90°$ and increases when increasing the inclination angle in the range of $270° \le \gamma \le 360°$. In the range of $90° \le \gamma \le 270°$ the Nusselt number varies sinusoidally as the inclination angle increases for the left or the right side of the heater source.

Besides, it is observed that the inclination angle is a key parameter for the calculation of heat transfer in the three sides of the source heater.

EFFECT OF THE HEATER DIMENSIONLESS HEIGHT (δ)

The effect of the heater dimensionless height (δ) on the isotherms and streamlines is demonstrated in Figures 6. In this section the heater dimensionless height is varied from 0.1 to 0.5 and its width is fixed at $\varepsilon = 0.2$ in the middle of the incinerator for all simulations. For all considered Rayleigh numbers (Ra=10^3-10^6) the isotherms and flow structures exhibits a symmetrical patterns from either sides of the heater as shown in Figures 6 (a, b). For Rayleigh numbers 10^3 and 10^4 (Figure 8) isotherms are parallel to the heater vertical walls. This behavior is more pronounced with the augmentation of the heater dimensionless height. At the heater to facet, isotherms are also parallel to the horizontal surface. The distance between isotherms decreases by increasing heater height δ. Two symmetric counter rotating cells are formed. The right cell is rotating clockwise and the left one is rotating anti-clockwise.

For Rayleigh numbers 10^5 and 10^6 (Figure 9), isotherms are parallel to the heater vertical walls and are very smoothed near the vertical walls. However for the top face of the heater, isotherms have a parabolic shape. This parabolic shape is well shown with increasing the Rayleigh number. For $\delta = 0,3$ and Ra=10^6, isotherms *θ=0.05* are perpendicular to the top face of the incinerator which is adiabatic. Increasing δ from 0.3 to 0.4 at Ra=10^6, the isotherms *θ=0.05* is at a position equal to 0.82; this can be explained by the stream function where we can see the formation of two cells on the top face of the heater source which are counter-rotating. The isotherms shape is reversed from the top of the incinerator to top side of the heater source. The thermal boundary layer thickness at the bottom side of heater source is decreased. This can be explained by the formation of two new contrarotative cells at the top face of the heater. These two cells contribute to the redistribution of energy to the left and right inclined walls and minimize the heat transfer to the top of the incinerator. Therefore on the two inclined sides of the incinerator the thermal boundary layer thickness decreases also.

Figure 10 shows that the average Nusselt number from the heater left side increases as the relative heat source height increases. This is evident because if the height δ is increased, more energy is introduced to the medium.

EFFECT OF THE RELATIVE HEATER DIMENSIONLESS WIDTH

Figures 7(a, b and c) show respectively the effect of relative heat source width on isotherms, streamlines and average Nusselt number for Ra=10^3-10^6 and $\varepsilon = 0,02 - 0,8$ in the case of pure water. The height of the heat source δ is maintained constant at 0.2.

Figures 7(a and b) demonstrate that the heater dimensionless width increase (with Ra=10^3-10^5) leads to formation of two symmetric cells which occupy the whole of the free space of the incinerator. Isotherms are normal to the adiabatic bottom incinerator wall and are tightened near the heater vertical sides.

For Ra=10^6 and $\delta = 0.4$ the symmetry of isotherms is broken, it is well pronounced for $\delta = 0.6$ where we can see that the two symmetric cells are broken to give four cells; one big cell situated at the top side of that heater and three other little eddies two on the right side and the third at the left side of the incinerator. The symmetry of isotherms is also broken and we can see the formation of thin boundary layer on the faces of the heater block and on the cold inclined walls of the incinerator.

For Ra=10^6 and $\varepsilon = 0.8$, Figure 12 shows the formation of six eddies occupying the whole area of the incinerator, results are quasi-symmetric and energy is transferred to the total area of the studied medium which gives also quasi-symmetric isotherms. The regime is unsteady due to the Rayleigh-Bénard like situation.

Figure 13 shows the effect of relative heat source width on average Nusselt number on the left side of the hot source. One can see easily that if the relative height ε is inferior to 0.6 and Ra=10^3-10^4, the average Nusselt number increases slightly with increasing relative heat source.

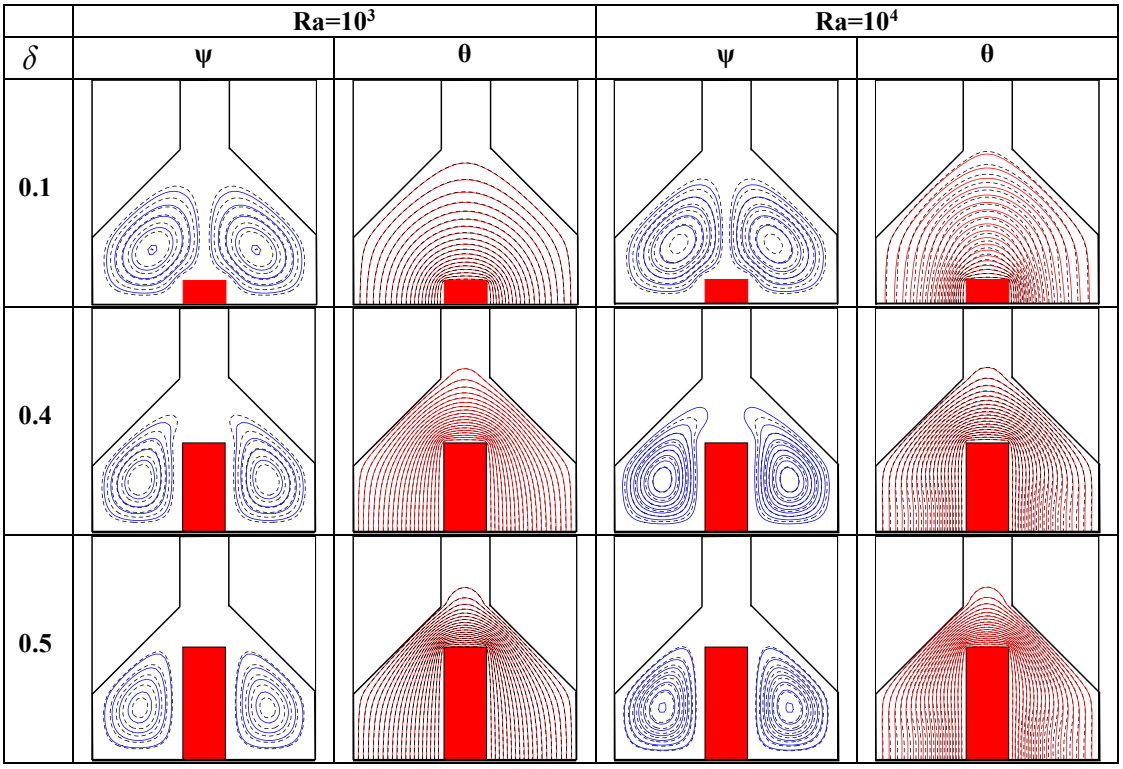

Figure 8 Effect of relative heat source height δ on streamlines and isotherms for Ra = 10^3 and 10^4 and ε=0.2 (─ Base fluid; ---nanofluid).

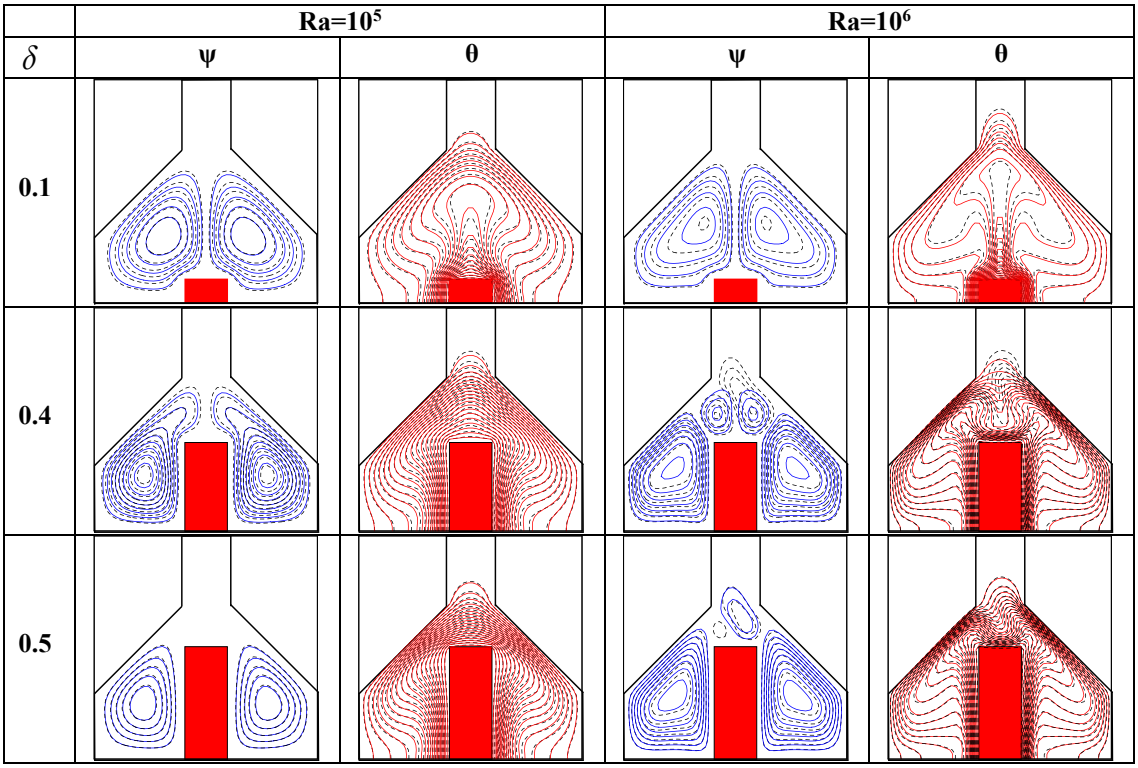

Figure 9. Effect of relative heat source height δ on streamlines and isotherms for Ra = 105 and 106 and ε=0.2 (─Base fluid; ---nanofluid).

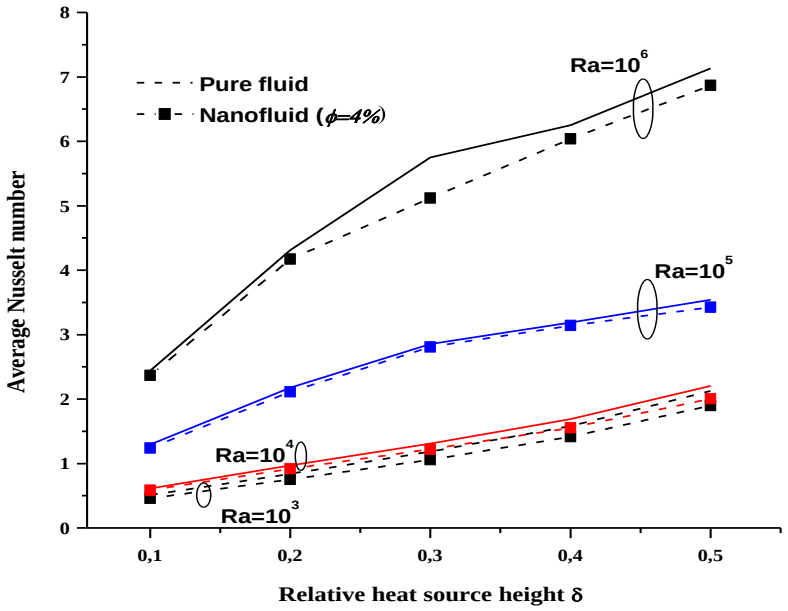

Figure 10. Effect of relative heat source height δ on average Nusselt number on the left side of the hot source for Ra = 10^3 - 10^6 and ε=0.2 (─Base fluid; ---nanofluid, $\phi = 4\%$).

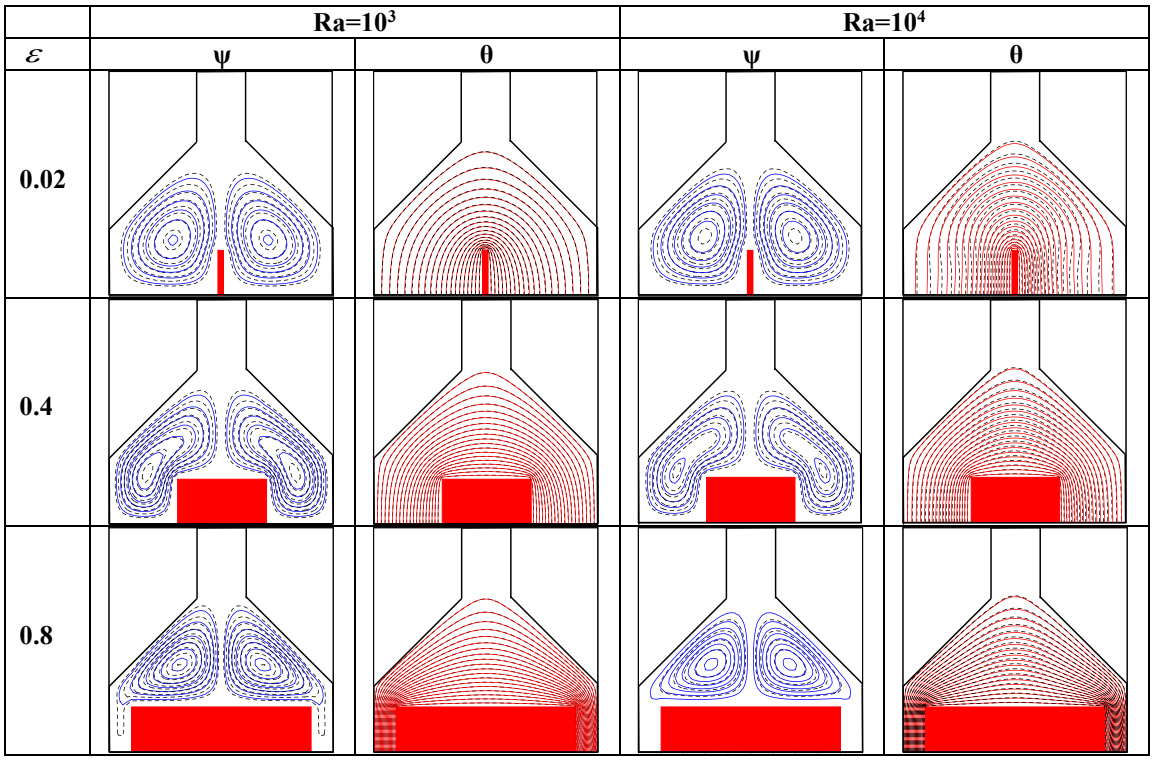

Figure 11. Effect of relative heat source width on streamlines and isotherms for Ra = 10^3 and 10^4 and δ=0.4 (─ Base fluid; ---nanofluid,).

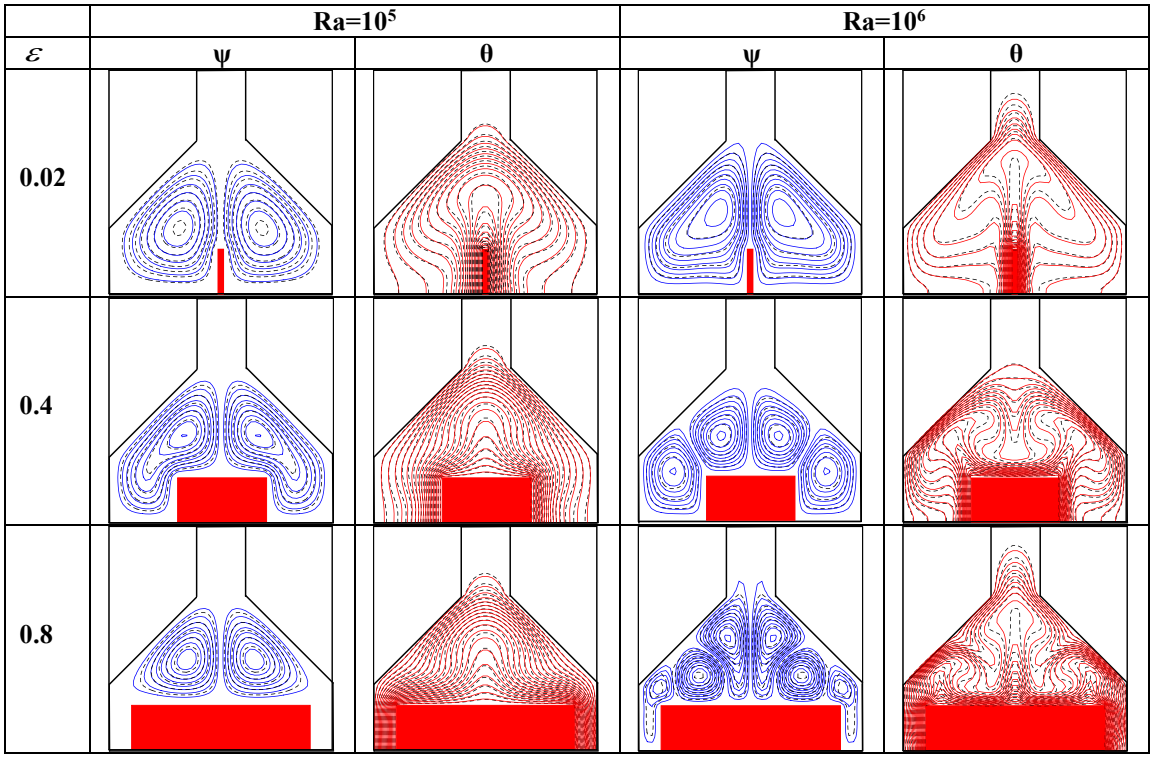

Figure 12. Effect of relative heat source width on streamlines and isotherms for Ra = 10^5 and 10^6 and δ=0.4 (─ Base fluid; ---nanofluid,).

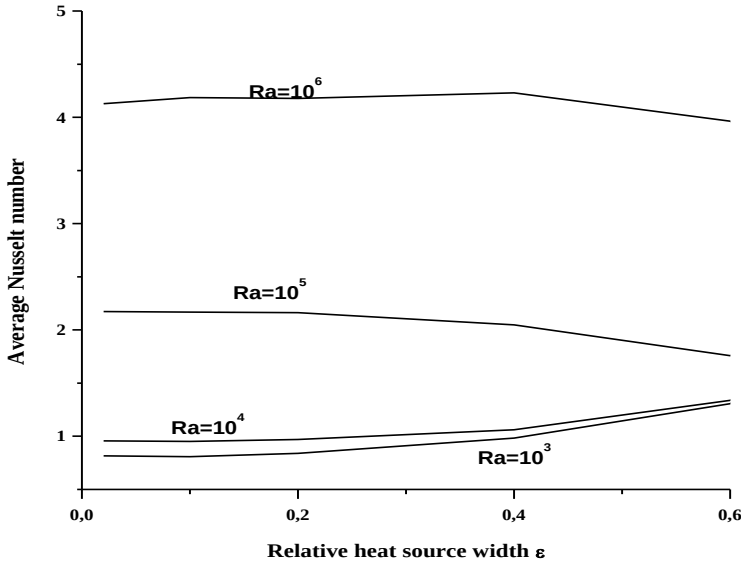

Figure 13. Effect of relative heat source width on average Nusselt number on the left side of the hot source Ra = 10^3 - 10^6 and δ=0.4 (─Base fluid; ---nanofluid, $\phi = 4\%$).

EFFECT OF THE HOT BLOCK POSITION

Figure 14 presents the effect of heat source positions on isotherms and streamlines for pure water and nanofluid for Ra=10^5. Evidently, one can say that moving the hot block toward the vertical cold side walls leads to symmetry breaking of the thermal and flow structures. At a middle position we note the formation of two cells. The lower is due to the like heated differentially cavity where intensively the heat transfer was verified and proved to increase significantly. The upper cell is due the like Rayleigh-Bénard convection. The thermal and flow structures in the presented three cases are significantly changed and the heat transfer is decreased by approaching

the incinerator side wall. This can be explained by the fact that the left wall of the hot block will be inactive and then less heat will be transferred to the fluid.

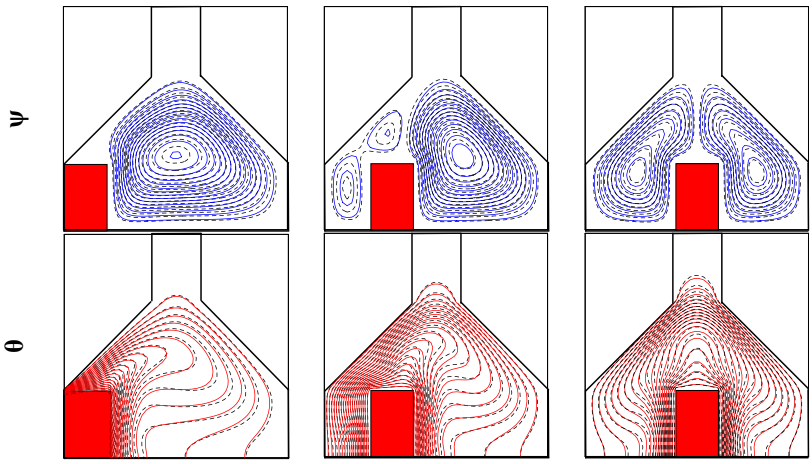

Figure 14. Effect heat source position on isotherms and streamlines for Ra = 10^5 and δ=0.4, ε=0.2 (─Base fluid; ---nanofluid).

CONCLUSION

Natural convection flow and heat transfer enhancement by Al_2O_3 nanosuspensions in an incinerator shaped enclosure containing a rectangular hot block is investigated in the present study. An indepth analysis of the monitoring parameters effects on the flow and thermal structures and the heat transfer enhancement is conducted by help of a SRT thermal lattice Boltzmann model.

From this study, the following conclusions are drawn:

1. Based on the quantitative and qualitative validation, the excellent agreement between ours results and former experimental and numerical data let us to rely on the powerfulness of the LB method to scrutinize such a two-phase like problem.
2. The Rayleigh number increase enhances for about three times the heat transfer for both pure fluid and nanofluid.
3. The addition of nanoparticles to the base fluid leads to the decrease of the activity of the fluid motion measured by the stream-function magnitude and causes a substantial increase in the heat transfer rate.
4. The inclination angle of the incinerator is found to be a key parameter to control the heat transfer for both pure water and nanofluid. The tilting angle affects significantly the heat transfer for the heater three walls.
5. The heat source tallness increase enhances the heat transfer for all its tested values and all Rayleigh numbers. However, the relative heat source width plays opposite role for dimensionless values superior to 0.4.

NOMENCLATURE

d_p	Diameter of particle, *nm*
k	Thermal conductivity, *W/m.K*
Ma	Mach number
Nu	Local Nusselt number
Pr	Prandtl number
Ra	Rayleigh number
T	Temperature, *K*
$\mathbf{u}(u,v)$	Velocities, m/s
$\mathbf{x}(x,y)$	Lattice coordinates, *m*
H	height of cavity, *m*

Greek symbols

α	Thermal diffusivity, m^2/s
β	Thermal expansion coefficient, K^{-1}

k_b Boltzmann constant, $J.\ K^{-1}$
Δx Lattice spacing, m
Δt Time increment, s
ϕ Solid volume fraction
μ Dynamic viscosity, $kg/m.s$
ρ Fluid density , kg/m^3
θ Non-dimensional temperature
ν Kinematic viscosity, m^2/s

Subscript

c cold
f fluid
h hot
nf nanofluid
p particle

REFERENCES

[1] Khaled, A. R. A., Siddique, M., Abdulhafiz, N. I., & Boukhary, A. Y. (2010). Recent advances in heat transfer enhancements: A review report. International Journal of Chemical Engineering.
[2] Bergles, A. E., (1998). Handbook of Heat Transfer, McGraw-Hill, New York, NY, USA, 3rd edition.
[3] Choi, S. U., & Eastman, J. A. (1995). Enhancing thermal conductivity of fluids with nanoparticles (No. ANL/MSD/CP--84938; CONF-951135--29). Argonne National Lab., IL (United States).
[4] Mahbubul, I. M., Saidur, R., & Amalina, M. A. (2012). Latest developments on the viscosity of nanofluids. International Journal of Heat and Mass Transfer, 55(4), 874-885.
[5] Shanbedi, M., Amiri, A., Heris, S. Z., & Kazi, S. N. (2015). Basic Principles and Modern Aspects.
[6] Cheikh, N. B., Chamkha, A. J., & Beya, B. B. (2009). Effect of inclination on heat transfer and fluid flow in a finned enclosure filled with a dielectric liquid. Numerical Heat Transfer, Part A: Applications, 56(3), 286-300.
[7] Abbassi, M. A., Mliki, B., & Djebali, R. (2017). Lattice Boltzmann Method for Simulation of Nanoparticle Brownian Motion and Magnetic Field Effects on Free Convection in A Nanofluid-filled Open Cavity with Heat Generation/Absorption and Non Uniform Heating on the Left Solid Vertical Wall.
[8] Oztop, H. F., Selimefendigil, F., Abu-Nada, E., & Al-Salem, K. (2016). Recent developments of computational methods on natural convection in curvilinear shaped enclosures. Journal of Thermal Engineering, 2(2),693-698.
[9] Moumni, H., Welhezi, H., Djebali, R., & Sediki, E. (2015). Accurate finite volume investigation of nanofluid mixed convection in two-sided lid driven cavity including discrete heat sources. Applied Mathematical Modelling, 39(14),4164-4179.
[10] Mahfoud, B., & Bendjaghlouli, A. (2018). Natural Convection of a Nanofluid in a Conical Container. Journal of Thermal Engineering, 4(1), 1713-1723.
[11] Hassan, H. (2014). Heat transfer of Cu–water nanofluid in an enclosure with a heat sink and discrete heat source. European Journal of Mechanics-B/Fluids, 45, 72-83.
[12] Öztop, H. F., Estellé, P., Yan, W. M., Al-Salem, K., Orfi, J., & Mahian, O. (2015). A brief review of natural convection in enclosures under localized heating with and without nanofluids. International Communications in Heat and Mass Transfer, 60, 37-44.
[13] Kaluri, R. S., Basak, T., & Roy, S. (2010). Heatline approach for visualization of heat flow and efficient thermal mixing with discrete heat sources. International Journal of Heat and Mass Transfer, 53(15-16), 3241-3261.
[14] Aminossadati, S. M., & Ghasemi, B. (2009). Natural convection cooling of a localised heat source at the bottom of a nanofluid-filled enclosure. European Journal of Mechanics-B/Fluids, 28(5), 630-640.
[15] Mussa, M. A., Abdullah, S., Azwadi, C. N., & Muhamad, N. (2011). Simulation of natural convection heat transfer in an enclosure by the lattice-Boltzmann method. Computers & Fluids, 44(1), 162-168.
[16] Paroncini, M., & Corvaro, F. (2009). Natural convection in a square enclosure with a hot source. International journal of thermal sciences, 48(9), 1683-1695.
[17] Chen, S., & Doolen, G. D. (1998). Lattice Boltzmann method for fluid flows. Annual review of fluid mechanics, 30(1),329-364.
[18] Djebali, R., El Ganaoui, M., & Pateyron, B. (2012). A lattice Boltzmann-based investigation of powder in-flight characteristics during APS process, part I: modelling and validation. Progress in Computational Fluid Dynamics, an International Journal, 12(4), 270-278.
[19] Dixit, H. N., & Babu, V. (2006). Simulation of high Rayleigh number natural convection in a square cavity

using the lattice Boltzmann method. International journal of heat and mass transfer, 49(3-4), 727-739.
[20] Patankar, S. (1980). Numerical heat transfer and fluid flow. CRC press.
[21] McNamara, G. R., & Zanetti, G. (1988). Use of the Boltzmann equation to simulate lattice-gas automata. Physical review letters, 61(20), 2332.
[22] Lai, F. H., & Yang, Y. T. (2011). Lattice Boltzmann simulation of natural convection heat transfer of Al2O3/water nanofluids in a square enclosure. International Journal of Thermal Sciences, 50(10), 1930-1941.